

Calculations of Chern number: equivalence of real-space and twisted-boundary-condition formulae

Ling Lin^{1,2}, Yongguan Ke³, Li Zhang^{1,2}, and Chaohong Lee^{1,2,4*}

¹*Institute of Quantum Precision Measurement, State Key Laboratory of Radio Frequency Heterogeneous Integration, Shenzhen University, Shenzhen 518060, China*

²*College of Physics and Optoelectronic Engineering, Shenzhen University, Shenzhen 518060, China*

³*Laboratory of Quantum Engineering and Quantum Metrology, School of Physics and Astronomy, Sun Yat-Sen University (Zhuhai Campus), Zhuhai 519082, China and*

⁴*Quantum Science Center of Guangdong-Hongkong-Macao Greater Bay Area (Guangdong), Shenzhen 518045, China*

(Dated: August 28, 2023)

Chern number is a crucial invariant for characterizing topological feature of two-dimensional quantum systems. Real-space Chern number allows us to extract topological properties of systems without involving translational symmetry, and hence plays an important role in investigating topological systems with disorder or impurity. On the other hand, the twisted boundary condition (TBC) can also be used to define the Chern number in the absence of translational symmetry. Here we study the relation between these different definitions of Chern number. In the thermodynamic limit, from the perturbative nature of the twist angles under the uniform gauge of TBC, we derive the two real-space formulae (the non-commutative Chern number and the Bott index formula) from the TBC formula by keeping the leading orders of involved eigenstates and operators. This means the equivalence of the two real-space formulae and the TBC formula for calculating Chern number. In further, we numerically verify the equivalence via the well-known Haldane model.

I. INTRODUCTION

Topological band theory has achieved great success in characterizing the topological nature of quantum matters in the past decades [1–4]. Beyond the well-known spontaneous breaking theory, topological quantum states are classified by intrinsic topological invariants [4, 5]. In the context of band theory, topological invariants are usually defined on the Bloch manifold. A fascinating nature of topological quantum state is that it is immune to perturbations, i.e. disorder and impurity, provided that the spectral gap and the underlying symmetry are preserved. However, the translational symmetry will be broken in a spatially disordered system, invalidating the band structure. In this situation, the topological band theory fails to give the topological invariant in systems without translational symmetry.

To characterize the topological nature in the presence of disorder, one may use the twisted boundary condition (TBC) to formulate topological invariants [6–11]. One of the prominent features of the TBC is that it operates in real space. This method works in quasi-periodic boundary condition and does not require any translational symmetry. Physically, topological invariants are closely related to the system’s response of current to the external perturbation. The TBC is equivalent to piercing magnetic flux through the system [7, 12, 13], which results in adiabatic currents in the system [14]. Hence, one is able to compute the corresponding response of current in the system to obtain the topological invariant, e.g. the quantum Hall conductance [7, 8, 15] and polarization

[6, 9, 16–18]. The twist angle is related to the quasi momentum of the eigenstate under certain gauge choice in disorder-free system, connecting the topological invariant defined through quasi momenta and twist angles [19].

Recently, the real-space formula of topological invariant draws many attentions. Unlike the momentum-space topological invariant that are defined on Brillouin manifold, one can construct topological invariants directly in real space, allowing computation without translational symmetry. Roughly speaking, the real-space formula of topological invariant can be classified into two types, (i) the non-commutative form [20–24] and (ii) the Bott index form [25–29]. In 1D topological insulators with chiral symmetry, the winding number can be well expressed by these two methods in real space [11, 30]. Moreover, in 1D systems, they are proved to be equivalent to the winding number defined through the TBC in the thermodynamic limit, and hence these two real-space formulae are also equivalent [11]. In 2D Chern insulator, the real-space Chern number is also found to possess the non-commutative form and the Bott index form. Both methods have been extensively used in studying disorder effect to topological insulators. However, it is still unclear whether the real-space formulae of Chern number can be related to the Chern number defined via the TBC.

In this article, we show that the Chern number defined via the TBC and the two real-space formulae (the non-commutative method and the Bott index method) are equivalent in the thermodynamic limit. The key point of the proof is to make use of the perturbative nature of the twist angle in TBC and expand operators and eigenstates up to the first order of θ_j/L_j with L_j being the number of cells in $j = x, y$ direction. With the perturbative analysis, the Chern number defined via TBC is reduced to the real-space formulae of Chern number. We also note that

* Email: chleecn@szu.edu.cn, chleecn@gmail.com

the Berry curvature defined via TBC becomes constant in the thermodynamic limit. In finite systems, the flatness of the Berry curvature will affect the accuracy of the non-commutative method, while the Bott index method is immune to the non-flat effects. To verify our argument, we present numerical calculations for the Haldane model. We compute the flatness of Berry curvature defined via TBC, and show that it tends to be a constant in the thermodynamic limit. We also numerically verify the equivalence of Chern number given by non-commutative method and the Bott index method.

The rest of this paper is organized as follows: In Sec. II, we briefly introduce the Chern number defined via the TBC. We consider a non-interacting system and target gapped eigenstates. In Sec. III, we perform numerical calculations for the Haldane model to verify our arguments, including the flatness of Berry curvature and the calculation of Chern number in real space. In Sec. IV, we briefly summarize and discuss the results.

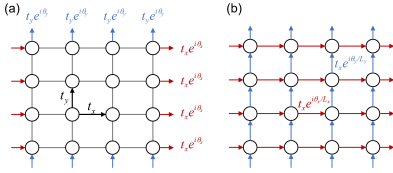


FIG. 1. Schematic illustration of the TBC in a 2D simple lattice. In both configurations, edges are glued together in the same manner as the periodic boundary condition. (a) is a general form of the TBC. The gauge field only appears at the boundary, and the particle gains extra phase when it tunnels through the boundary, as indicated by color arrows. (b) is transformed from (a) via a large gauge transformation. The gauge field distributes uniformly throughout the bulk, and the field strength is diluted.

II. CHERN NUMBER: FROM TWISTED BOUNDARY CONDITION TO REAL-SPACE FORMULAE

A. Chern number defined via twisted boundary condition

In this section, we introduce the TBC and the Chern number defined through TBC. Under the TBC, the lattice's edges are “glued” together pairwise as a 2D torus, just like the periodic boundary condition (PBC). The core is that we enforce particles to gain an extra phase θ after they tunnel through the boundary, as demonstrated in Fig. 1 (a). Apparently, $\theta = 0$ corresponds exactly to the PBC.

Next, we consider a non-interacting 2D system under TBC. The system's Hamiltonian satisfies $\hat{H}(\theta_x + 2\pi, \theta_y) = \hat{H}(\theta_x, \theta_y + 2\pi) = \hat{H}(\theta_x, \theta_y)$. Then, we target a set of single-particle eigenstates that are gapped to other eigenstates. Note that, if translation

symmetry is preserved, these eigenstates correspond to gapped bands. For simplicity, we collect these eigenstates and introduce the following notation

$$\Psi_{\theta} = (|\psi_1(\theta)\rangle \ |\psi_2(\theta)\rangle \ \cdots \ |\psi_N(\theta)\rangle), \quad (1)$$

where $|\psi_{\mu}(\theta)\rangle$ is the μ -th eigenstate of the Hamiltonian under TBC, and N is the total number of these targeted states. There is $\Psi_{\theta}^{\dagger} \Psi_{\theta} = I_N$ with I_N being the $N \times N$ identity matrix, and the projector of this subspace can be expressed as $\Psi_{\theta} \Psi_{\theta}^{\dagger} = \sum_{\mu} |\psi_{\mu}(\theta)\rangle \langle \psi_{\mu}(\theta)|$. These targeted states are assumed to remain gapped for $\theta_x, \theta_y \in [0, 2\pi]$, which is true in the thermodynamic limit. The Chern number of these targeted states can be expressed through the twist angles (θ_x, θ_y) [8]:

$$C_{\text{TBC}} = \frac{1}{2\pi} \int_0^{2\pi} \int_0^{2\pi} \text{Tr} [\mathcal{F}(\theta)] d^2\theta, \quad (2)$$

in which $\mathcal{F}(\theta)$ is the non-Abelian Berry curvature

$$\begin{aligned} \mathcal{F}(\theta) &= \partial_{\theta_x} \mathcal{A}_y(\theta) - \partial_{\theta_y} \mathcal{A}_x(\theta) + [\mathcal{A}_x(\theta), \mathcal{A}_y(\theta)], \\ \mathcal{A}_j(\theta) &= -i \Psi_{\theta}^{\dagger} \partial_{\theta_j} \Psi_{\theta}, \quad j = x, y. \end{aligned} \quad (3)$$

Note that $\mathcal{A}_j(\theta)$ is a N -by- N matrix. The minus sign in $\mathcal{A}_j(\theta)$ is related to the sign of twist angles defined in the TBC. Eq. (2) can well capture the topological property (quantum Hall conductance) of the system [8].

Alternatively, by introducing the projector that projects onto the targeted states $\hat{P}_{\theta} = \Psi_{\theta} \Psi_{\theta}^{\dagger}$, the Chern number can be equivalently expressed as [31]

$$C_{\text{TBC}} = \frac{1}{2\pi i} \int_0^{2\pi} \int_0^{2\pi} \text{Tr} \left(\hat{P}_{\theta} \left[\partial_{\theta_x} \hat{P}_{\theta}, \partial_{\theta_y} \hat{P}_{\theta} \right] \right) d^2\theta. \quad (4)$$

Given that the targeted states are gapped, the projector will finally return to itself after the twist angle changes 2π , that is: $\hat{P}_{\theta+2\pi\hat{e}_j} = \hat{P}_{\theta}$, with \hat{e}_j the unit vector along $j = x, y$ direction. In other words, the projector is a periodic function of twist angles.

B. Large gauge transformation and uniform gauge

Under the TBC, the extra phase gained by particle at the boundary can be regarded as a result of gauge field, and therefore there exists gauge freedom. It is beneficial to transform the gauge field at the boundary to a uniformly distributed gauge field throughout the whole system. By introducing the twist operator [32, 33]

$$\hat{U}_{\theta} = \exp \left(i \frac{\theta_x}{L_x} \hat{r}_x + i \frac{\theta_y}{L_y} \hat{r}_y \right), \quad (5)$$

where $\hat{r}_j = \sum_{\mathbf{r}} r_j \hat{n}_{\mathbf{r}}$ is the position operator in $j = x, y$ direction, we can bring the original system under TBC to

a unitarily equivalent system via the large gauge transformation

$$\tilde{H}(\boldsymbol{\theta}) = \hat{U}_{\boldsymbol{\theta}} \hat{H}(\boldsymbol{\theta}) \hat{U}_{\boldsymbol{\theta}}^{-1}. \quad (6)$$

Here, $\tilde{H}(\boldsymbol{\theta})$ indicates the transformed Hamiltonian. The two unitarily equivalent systems are illustrated in Fig. 1. To distinguish these two gauges, we use the tilde notation to stress that the operator (eigenstate) is under the gauge that the twist angles uniformly distribute. For convenience, we will call this gauge the *uniform gauge*, while the original TBC is called *boundary gauge*. In this case, the Chern number can still be written as the same form

$$\tilde{C}_{\text{TBC}} = \frac{1}{2\pi} \int_0^{2\pi} \int_0^{2\pi} \text{Tr} \left[\tilde{\mathcal{F}}(\boldsymbol{\theta}) \right] d^2\boldsymbol{\theta}, \quad (7)$$

and

$$\begin{aligned} \tilde{\mathcal{F}}(\boldsymbol{\theta}) &= \partial_{\theta_x} \tilde{\mathcal{A}}_y(\boldsymbol{\theta}) - \partial_{\theta_y} \tilde{\mathcal{A}}_x(\boldsymbol{\theta}) + \left[\tilde{\mathcal{A}}_x(\boldsymbol{\theta}), \tilde{\mathcal{A}}_y(\boldsymbol{\theta}) \right], \\ \tilde{\mathcal{A}}_j(\boldsymbol{\theta}) &= -i \tilde{\Psi}_{\boldsymbol{\theta}}^\dagger \partial_{\theta_j} \tilde{\Psi}_{\boldsymbol{\theta}}, \quad j = x, y. \end{aligned} \quad (8)$$

Note that $\tilde{\Psi}_{\boldsymbol{\theta}} = \hat{U}_{\boldsymbol{\theta}} \Psi_{\boldsymbol{\theta}}$. It can be proved that Eq. (3) and Eq. (8) are equivalent: $\tilde{C}_{\text{TBC}} = C_{\text{TBC}}$, see the proof in A. Similar to Eq. 4, we can formulate the Chern number through the projector $\tilde{P}_{\boldsymbol{\theta}} = \tilde{\Psi}_{\boldsymbol{\theta}} \tilde{\Psi}_{\boldsymbol{\theta}}^\dagger$

$$\tilde{C}_{\text{TBC}} = \frac{1}{2\pi i} \int_0^{2\pi} \int_0^{2\pi} \text{Tr} \left(\tilde{P}_{\boldsymbol{\theta}} \left[\partial_{\theta_x} \tilde{P}_{\boldsymbol{\theta}}, \partial_{\theta_y} \tilde{P}_{\boldsymbol{\theta}} \right] \right) d^2\boldsymbol{\theta}, \quad (9)$$

in which the projector satisfies

$$\tilde{P}_{\boldsymbol{\theta}} = \hat{U}_{\boldsymbol{\theta}} \hat{P}_{\boldsymbol{\theta}} \hat{U}_{\boldsymbol{\theta}}^{-1}. \quad (10)$$

In the transformed Hamiltonian (6), the twist angle θ is transformed to distribute in all tunneling terms of the system. Particles gain a “diluted” phase factor during the tunneling process, that is

$$\hat{U}_{\boldsymbol{\theta}} \hat{c}_{\mathbf{r}+\mathbf{d}}^\dagger c_{\mathbf{r}} \hat{U}_{\boldsymbol{\theta}}^{-1} = e^{i \left(\frac{\theta_x}{L_x} d_x + \frac{\theta_y}{L_y} d_y \right)} \hat{c}_{\mathbf{r}+\mathbf{d}}^\dagger c_{\mathbf{r}}. \quad (11)$$

When the tunneling range is finite $d_{x,y} \ll L_{x,y}$, the twist angle appears as θ_j/L_j , $j = x, y$, which can be considered as a perturbation. Hence, it is desirable to expand operators or eigenstates up to the first order of $1/L_j$ for sufficiently large system. This also explains why the gapped eigenstate will remain gapped for arbitrary $\theta_{x,y}$ in the thermodynamic limit $L_{x,y} \rightarrow \infty$, as the energy gap is only weakly perturbed. In next subsections, we shall make use of the perturbative nature of the twist angle to derive the two real-space formulae of the Chern number.

C. Real-space Chern number via non-commutative method

In this subsection, we derive the the non-commutative real-space formula of the Chern number. This formula

is firstly proposed in Ref. [20, 23], which is based on the momentum-space formula of the Chern number [34]

$$C = \frac{1}{2\pi i} \int_{B.Z.} \text{Tr} \left\{ \hat{\mathbb{P}}(\mathbf{k}) \left[\partial_{k_x} \hat{\mathbb{P}}(\mathbf{k}), \partial_{k_y} \hat{\mathbb{P}}(\mathbf{k}) \right] \right\} d^2\mathbf{k}, \quad (12)$$

where $\hat{\mathbb{P}}(\mathbf{k}) = \sum_{n \in \text{occ.}} |u_{\mathbf{k}}^n\rangle \langle u_{\mathbf{k}}^n|$ is the projector onto Bloch states of occupied bands with momentum \mathbf{k} . To derive the real-space formula, their idea is to transform the partial derivative and the integral in Brillouin zone to real space [20, 23], which leads to the following non-commutative form of Chern number

$$C = -2\pi i \sum_{\alpha} \langle \mathbf{r}_0, \alpha | \hat{P} \left[\left[\hat{r}_x, \hat{P} \right], \left[\hat{r}_y, \hat{P} \right] \right] | \mathbf{r}_0, \alpha \rangle, \quad (13)$$

where \hat{P} is the projector onto eigenstates in occupied bands, and $|\mathbf{r}_0, \alpha\rangle$ is the real-space basis denoting the cell at \mathbf{r}_0 and α is the label of internal orbits within the cell. This formula has been successfully applied to various systems [20, 35, 36].

Next, we would like to show that the non-commutative Chern number can be equivalently derived through the TBC Chern number [Eq. (9)]. For this purpose, we will make use of the perturbative nature of the twist angle under the uniform gauge. Firstly, we expand the projector in terms of θ_j/L_j up to the first order near $\boldsymbol{\theta} = 0$:

$$\begin{aligned} \tilde{P}_{\boldsymbol{\theta}} &= \hat{P} + \frac{\theta_x}{L_x} \frac{\partial \tilde{P}_{\boldsymbol{\theta}}}{\partial (\theta_x/L_x)} \Big|_{\boldsymbol{\theta}=0} + \frac{\theta_y}{L_y} \frac{\partial \tilde{P}_{\boldsymbol{\theta}}}{\partial (\theta_y/L_y)} \Big|_{\boldsymbol{\theta}=0} \\ &\quad + O \left(\frac{1}{L_x^2} + \frac{1}{L_y^2} \right), \end{aligned} \quad (14)$$

where we use the fact that $\hat{P} = \tilde{P}_{\boldsymbol{\theta}=0}$ since $\boldsymbol{\theta} = 0$ corresponds to general systems under PBC. Substituting Eq. (14) into Eq. (9) and keeping up to the leading order lead to:

$$\tilde{P}_{\boldsymbol{\theta}} \left[\partial_{\theta_x} \tilde{P}_{\boldsymbol{\theta}}, \partial_{\theta_y} \tilde{P}_{\boldsymbol{\theta}} \right] \approx \hat{P} \left[\left(\partial_{\theta_x} \tilde{P}_{\boldsymbol{\theta}} \right) \Big|_{\boldsymbol{\theta}=0}, \left(\partial_{\theta_y} \tilde{P}_{\boldsymbol{\theta}} \right) \Big|_{\boldsymbol{\theta}=0} \right] \quad (15)$$

which is independent on the twist angle. This fact implies that the trace of the Berry curvature defined through TBC should be also independent on the twist angle $\text{Tr}[\tilde{\mathcal{F}}(\boldsymbol{\theta})] \approx \text{constant}$ in the thermodynamic limit $L_x, L_y \rightarrow \infty$. We shall examine this point in Sec. III.

Since the trace of the Berry curvature is a constant for sufficiently large systems, the Chern number [Eq. (9)] can be approximated without implementing integrations [37]:

$$\tilde{C}_{\text{TBC}} \approx -2\pi i \text{Tr} \left(\hat{P} \left[\left(\partial_{\theta_x} \tilde{P}_{\boldsymbol{\theta}} \right) \Big|_{\boldsymbol{\theta}=0}, \left(\partial_{\theta_y} \tilde{P}_{\boldsymbol{\theta}} \right) \Big|_{\boldsymbol{\theta}=0} \right] \right). \quad (16)$$

Next, we let $\theta_x = 2\pi, \theta_y = 0$, which maintains the perturbative condition since $2\pi/L_x \ll 1$. According to Eq. (10),

we find the following useful relation

$$\begin{aligned}\tilde{P}_{(2\pi,0)} &= \hat{P} + \frac{2\pi}{L_x} \frac{\partial \tilde{P}_{\theta}}{\partial (\theta_x/L_x)} \Big|_{\theta=0} + O\left(\frac{1}{L_x^2}\right) \quad (17) \\ &= \hat{U}_{2\pi}^x \hat{P} \left(\hat{U}_{2\pi}^x \right)^{-1},\end{aligned}$$

where we introduce the twist operator along single direction $\hat{U}_{\theta_j}^j \equiv \exp(i\theta_j \hat{r}_j/L_j)$, $j = x, y$ for simplicity. A similar result can be obtained by letting $\theta_x = 0, \theta_y = 2\pi$. Up to the first order of $1/L_j$, $j = x, y$, Eq. (17) provides a very convenient approach to approximate the partial derivative w.r.t. the twist angle:

$$\begin{aligned}\frac{2\pi}{L_j} \frac{\partial \tilde{P}_{\theta}}{\partial (\theta_j/L_j)} \Big|_{\theta=0} &= 2\pi \frac{\partial \tilde{P}_{\theta}}{\partial \theta_j} \Big|_{\theta=0} \\ &\approx \tilde{P}_{2\pi e_j} - \hat{P} \\ &= \hat{U}_{2\pi}^j \hat{P} \left(\hat{U}_{2\pi}^j \right)^{-1} - \hat{P}. \quad (18)\end{aligned}$$

Furthermore, by using the Baker-Campbell-Hausdorff formula, we have

$$e^{i\frac{2\pi}{L_j} \hat{r}_j} \hat{P} e^{-i\frac{2\pi}{L_j} \hat{r}_j} = \hat{P} + i\frac{2\pi}{L_j} [\hat{r}_j, \hat{P}] + O\left(\frac{1}{L_j^2}\right), \quad (19)$$

and therefore the partial derivative of the projector can be further written as

$$\frac{\partial \tilde{P}_{\theta}}{\partial \theta_j} \Big|_{\theta=0} \approx \frac{i}{L_j} [\hat{r}_j, \tilde{P}], \quad j = x, y. \quad (20)$$

By combining Eqs. (9), (15), (20), we consequently obtain the following real-space form of the Chern number

$$\begin{aligned}\tilde{C}_{\text{TBC}} &\approx \frac{2\pi i}{L_x L_y} \text{Tr} \left(\hat{P} \left[[\hat{r}_x, \hat{P}], [\hat{r}_y, \hat{P}] \right] \right) \\ &= \frac{2\pi i}{L_x L_y} \sum_{\mathbf{r}, \alpha} \langle \mathbf{r}, \alpha | \hat{P} \left[[\hat{r}_x, \hat{P}], [\hat{r}_y, \hat{P}] \right] | \mathbf{r}, \alpha \rangle. \quad (21)\end{aligned}$$

It can be found that this formula is quite similar to the non-commutative Chern number [Eq. (13)] proposed before (up to a minus sign, depending on the convention of the coordinate). A minor difference is that Eq. (13) performs trace only within a single cell, while Eq. (21) traces for all cells and then averages them. For clean systems with translation symmetry, one can easily deduce that these two approaches are well consistent. As for disordered system, they are also consistent if we average over many random realizations. If the system is inhomogeneous, i.e. a harmonic trap is imposed, it is more reasonable to consider an average over all sites. We also point out that the approximation in Eq. (18) is relatively rough in finite systems. One can use a higher-order finite difference method to gain a more accurate result, see details in B.

D. Real-space Chern number via Bott index method

In this section, we derive the Bott-index form of the real-space Chern number through the TBC. The Bott index form of the Chern number is proposed to efficiently calculate the intrinsic topological nature in real space [25–29, 38], and has been applied widely in various systems [39–44]. It is pointed out that the Bott index is equivalent to the quantum Hall conductance [45]. The Bott index is considered as a winding number index of matrices that almost represents the disk or annulus [27, 45]. For Chern insulators, the Bott index reads as

$$\text{Bott}(\mathcal{U}_x, \mathcal{U}_y) = \frac{1}{2\pi i} \text{tr} \left[\log \left(\mathcal{U}_x \mathcal{U}_y \mathcal{U}_x^\dagger \mathcal{U}_y^\dagger \right) \right], \quad (22)$$

where $\mathcal{U}_j = \Psi^\dagger \hat{U}_{2\pi}^j \Psi$, $j = x, y$. Here, the notation “ $\text{tr}()$ ” means the trace operation of the matrix, which implies the trace in the subspace spanned by targeted states.

Next, we show that the Bott index Chern number can be derived from the Chern number defined through TBC [Eq. (7)]. The idea is also to use the perturbative nature of the twist angle. However, to derive a Bott index form, we shall take another route. Firstly, it can be proved that the Chern number can be written as a winding of Berry phase (line integral) [31]

$$\tilde{C}_{\text{TBC}} = \frac{1}{2\pi} \int_0^{2\pi} d\theta_x \frac{\partial}{\partial \theta_x} \phi_{\text{Berry}}^y(\theta_x) \quad (23)$$

in which

$$\phi_{\text{Berry}}^y(\theta_x) = \int_0^{2\pi} d\theta_y \text{tr} \left[\tilde{\mathcal{A}}_y(\boldsymbol{\theta}) \right] \quad (24)$$

is the Berry phase along the y direction. Using the perturbative nature of the twist angle, one can obtain the Berry phase in real space via the following expression [19]

$$\begin{aligned}\phi_{\text{Berry}}^y(\theta_x) &= -i \text{tr} \left[\exp \left(\int_0^{2\pi} \tilde{\mathcal{A}}_x(\boldsymbol{\theta}) d\theta_y \right) \right] \\ &\approx -i \text{tr} \left\{ \log \left[\tilde{\Psi}_{(\theta_x, 0)}^\dagger \tilde{\Psi}_{(\theta_x, 2\pi)} \right] \right\} \\ &= -i \text{tr} \left\{ \log \left[\Psi_{(\theta_x, 0)}^\dagger \hat{U}_{2\pi}^y \Psi_{(\theta_x, 0)} \right] \right\}, \quad (25)\end{aligned}$$

where we have used the fact that $\tilde{\Psi}_{(\theta_x, 2\pi)} = \hat{U}_{2\pi}^y \tilde{\Psi}_{(\theta_x, 0)}$. The above formula can be equivalently formulated via the projected position operator $\hat{P}_y(\theta_x) \equiv \tilde{P}_{(\theta_x, 0)} \hat{U}_{2\pi}^y \tilde{P}_{(\theta_x, 0)}$ such that

$$\phi_{\text{Berry}}(\theta_x) \approx -i \text{Tr} \left[\log \left(\hat{P}_y(\theta_x) \right) \right]. \quad (26)$$

By differentiating Eq. (26) w.r.t. the twist angle θ_x , we find (see detailed derivation in D)

$$\frac{\partial}{\partial \theta_x} \phi_{\text{Berry}}(\theta_x) = -i \text{Tr} \left[\hat{P}_y(\theta_x)^\dagger \frac{\partial}{\partial \theta_x} \hat{P}_y(\theta_x) \right]. \quad (27)$$

Together with Eq. (23), one may find the Chern number is the winding number of projected position operator.

Next, we further treat the twist angle θ_x/L_x as a perturbation term, and expand the projected position operator $\hat{\mathcal{P}}_y(\theta_x)$ up to the first order

$$\hat{\mathcal{P}}_y(\theta_x) = \hat{\mathcal{P}}_y(0) + \theta_x \left[\frac{\partial}{\partial \theta_x} \hat{\mathcal{P}}_y(\theta_x) \right]_{\theta_x=0} + O\left(\frac{1}{L_x^2}\right). \quad (28)$$

This fact means, up to the first order of $1/L_x$, the Berry phase (polarization) along y direction is a linear function of θ_x , which is consistent with previous studies [46–48]. By substituting the expansion in Eq. (28) into Eq. (26) and integrating the twist angle θ_x , we find the Chern number can be approximated to

$$\tilde{C}_{\text{TBC}} = -i\text{Tr} \left\{ \hat{\mathcal{P}}_y(0)^\dagger \left[\frac{\partial}{\partial \theta_x} \hat{\mathcal{P}}_y(\theta_x) \right]_{\theta_x=0} \right\} + O\left(\frac{1}{L_x^2}\right). \quad (29)$$

Then, we can make use of the approximation

$$\hat{\mathcal{P}}_y(2\pi) - \hat{\mathcal{P}}_y(0) \approx 2\pi \left[\frac{\partial}{\partial \theta_x} \hat{\mathcal{P}}_y(\theta_x) \right]_{\theta_x=0}, \quad (30)$$

and then approximately we have

$$\tilde{C}_{\text{TBC}} \approx \frac{1}{2\pi i} \text{Tr} \left[\hat{\mathcal{P}}_y(0)^\dagger \hat{\mathcal{P}}_y(2\pi) - \hat{\mathcal{P}}_y(0)^\dagger \hat{\mathcal{P}}_y(0) \right]. \quad (31)$$

To obtain the Bott index form, we convert the trace operation (Tr) to the matrix trace (tr) in the subspace spanned by the targeted states

$$\begin{aligned} \text{Tr} \left[\hat{\mathcal{P}}_y(0)^\dagger \hat{\mathcal{P}}_y(2\pi) - \hat{\mathcal{P}}_y(0)^\dagger \hat{\mathcal{P}}_y(0) \right] \\ = \text{tr} \left(\mathcal{U}_y^\dagger \mathcal{U}_x \mathcal{U}_y \mathcal{U}_x^\dagger - \mathcal{U}_y^\dagger \mathcal{U}_y \right). \end{aligned} \quad (32)$$

In Eq. (32), we have used the fact that $\hat{\mathcal{P}}_y(2\pi) = \hat{U}_{2\pi}^x \hat{\mathcal{P}}_y(0) \left(\hat{U}_{2\pi}^x \right)^{-1}$ and $[\hat{U}_{2\pi}^x, \hat{U}_{2\pi}^y] = 0$. For gapped targeted states, matrices $\mathcal{U}_{x,y}$ are quasi-unitary $\mathcal{U}_y^\dagger \mathcal{U}_y \approx I_N$ (see proof in C), in which I_N is the $N \times N$ identity matrix in the subspace spanned by the targeted states. In practical calculations with finite length, one can perform the singular value decomposition (SVD) for these two matrices: $\mathcal{U}_{x,y} = \mathbf{U} \Sigma \mathbf{V}^{-1}$, in which $\mathbf{U}, \mathbf{V} \in \text{U}(\mathcal{N})$ are unitary matrices, and Σ is a diagonal matrix. The singular values are non-zero and close to identity as long as the targeted states are gapped. Then, one can enforce all singularity to be identity $\Sigma = I_N$, and then the unitarity of the matrix can be guaranteed: $\mathcal{U}_{x,y} = \mathbf{U} \mathbf{V}^{-1} \in \text{U}(\mathcal{N})$. Finally, given that $\mathcal{U}_y^\dagger \mathcal{U}_x \mathcal{U}_y \mathcal{U}_x^\dagger$ is close to the identity matrix, we can utilize the matrix logarithm and approximate Eq. (31) as:

$$\tilde{C}_{\text{TBC}} = \frac{1}{2\pi i} \text{tr} \left[\log \left(\mathcal{U}_y^\dagger \mathcal{U}_x \mathcal{U}_y \mathcal{U}_x^\dagger \right) \right], \quad (33)$$

which is consistent with Eq. (22). Note that the order of these matrices can be circularly permuted in 32 due

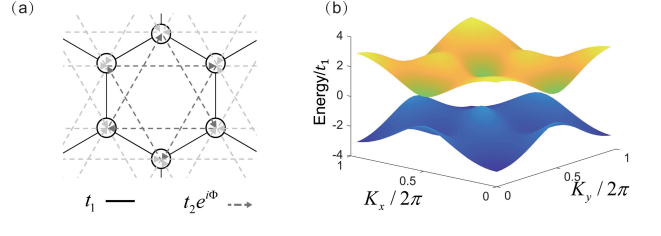


FIG. 2. (a) Schematic illustration of the tunneling relations within a single hexagon in Haldane model and (b) the typical band structure. The lattice constant is set to unity for convenience.

to the trace operation. The derivation is quite similar to the real-space representation of the winding number in Ref. [11]. Owing to the unitarity of the matrices $\mathcal{U}_{x,y}$, one can conclude that $\det \left(\mathcal{U}_y^\dagger \mathcal{U}_x \mathcal{U}_y \mathcal{U}_x^\dagger \right) \in \mathbb{R}$, and therefore the Chern number (Bott index) here should be strictly an integer.

III. APPLICATIONS IN THE HALDANE MODEL

In this section, we present some numerical calculations to verify our results, including the flatness of the Berry curvature defined through TBC and applications of the two real-space formulae of the Chern number. Here, we consider the celebrated Haldane model [49], which realizes the Chern insulator without requiring net magnetic field. The Haldane model has been experimentally simulated via ultracold atom platform [50, 51]. The Hamiltonian of Haldane model reads as

$$\hat{H}_0 = - \sum_{\langle \mathbf{r}, \mathbf{r}' \rangle} t_1 \hat{c}_{\mathbf{r}}^\dagger \hat{c}_{\mathbf{r}'} - \sum_{\langle\langle \mathbf{r}, \mathbf{r}' \rangle\rangle} t_2 e^{i\Phi_{\mathbf{r}, \mathbf{r}'}} \hat{c}_{\mathbf{r}}^\dagger \hat{c}_{\mathbf{r}'} + \text{H.c.}, \quad (34)$$

in which t_1 is the nearest-neighbor (NN) tunneling strength, t_2 is the next-nearest-neighbor (NNN) tunneling strength, and $\Phi_{\mathbf{r}, \mathbf{r}'}$ is the gauge field addressed to the NNN tunneling, as demonstrated in Fig. 2. Here $\langle \mathbf{r}, \mathbf{r}' \rangle$ and $\langle\langle \mathbf{r}, \mathbf{r}' \rangle\rangle$ respectively represent the NN sites and NNN sites. For simplicity, we let the energy difference between two sublattices be zero. By varying $|t_2/t_1|$ and the gauge field strength, the system exhibits topologically trivial or non-trivial phases. In what follows, we shall choose $t_1 = 1$, $t_2 = 0.5$, $\Phi = \pi/2$ to let the system reside in the topological non-trivial phase in the clean limit.

A. Flatness of the Berry curvature

In Sec. II B, we have shown that the trace of non-Abelian Berry curvature defined through the TBC should tends to be a constant in the thermodynamic limit. The flat Berry curvature allows us to compute the Chern number without integration, which is important to derive the

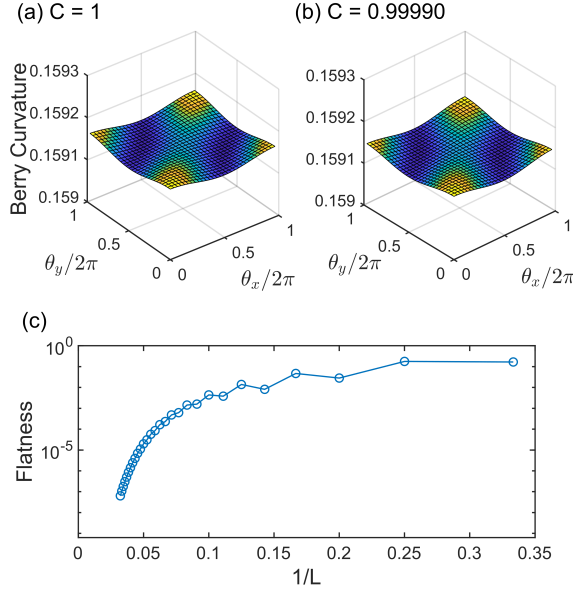


FIG. 3. Numerical computation of the Berry curvature defined through the TBC [Eq. (8)]. The Chern number is obtained by summing the Berry curvature $C = \frac{1}{2\pi} \sum_{\theta} \text{Tr} [\tilde{\mathcal{F}}(\theta)] \delta\theta_x \delta\theta_y$. We have used two different numerical methods to compute the Berry curvature: (a) the link variable method [Eq. (35)], and (b) the finite difference method [Eq. (37)] with 30×30 grid points. The system size is chosen as $L_x = L_y = 11$. (c) scaling of the flatness of Berry curvature [Eq. (38)] under different system sizes $L_x = L_y = L$. Other parameters are set to $t_1 = 1$, $t_2 = 0.5$, $\Phi = \pi/2$.

real-space Chern number. In this subsection, we shall verify this point numerically.

To compute the Berry curvature numerically through TBC, one should discretize the twist angle and use appropriate numerical method. Generally, one can adopt the link variable method [52]

$$\begin{aligned} \text{Tr} [\tilde{\mathcal{F}}(\theta)] \delta\theta_x \delta\theta_y &= \ln \det [\tilde{\Psi}_{(\theta_x, \theta_y)}^\dagger \tilde{\Psi}_{(\theta_x + \delta\theta_x, \theta_y)}] \\ &+ \ln \det [\tilde{\Psi}_{(\theta_x + \delta\theta_x, \theta_y)}^\dagger \tilde{\Psi}_{(\theta_x + \delta\theta_x, \theta_y + \delta\theta_y)}] \\ &+ \ln \det [\tilde{\Psi}_{(\theta_x + \delta\theta_x, \theta_y + \delta\theta_y)}^\dagger \tilde{\Psi}_{(\theta_x, \theta_y + \delta\theta_y)}] \\ &+ \ln \det [\tilde{\Psi}_{(\theta_x, \theta_y + \delta\theta_y)}^\dagger \tilde{\Psi}_{(\theta_x, \theta_y)}], \end{aligned} \quad (35)$$

which produces a gauge-invariant result.

Alternatively, based on Eq. (9), one can use the finite difference method to approximate the partial derivative

$$\partial_{\theta_j} \tilde{P}_{\theta} \approx \frac{\tilde{P}_{\theta + \delta\theta_j} - \tilde{P}_{\theta}}{|\delta\theta_j|}, \quad j = x, y, \quad (36)$$

and then we have

$$\text{Tr} [\tilde{\mathcal{F}}(\theta)] \approx \text{Tr} \left\{ \tilde{P}_{\theta} \left[\frac{\tilde{P}_{\theta + \delta\theta_x} - \tilde{P}_{\theta}}{|\delta\theta_x|}, \frac{\tilde{P}_{\theta + \delta\theta_y} - \tilde{P}_{\theta}}{|\delta\theta_y|} \right] \right\}. \quad (37)$$

It should be noted that the projector \tilde{P}_{θ} is gauge-invariant, and therefore Eq. (37) is gauge-invariant as well.

We then numerically compute the Berry curvature using these two methods, as shown in Fig. 3 (a-b). As expected, the Berry curvature defined through the TBC is very flat. By summing over all discretized terms, one will obtain the Chern number. It can be seen that the link variable method [Eq. (35)] strictly gives a integer Chern number, which is accurate, while the finite difference method [Eq. (37)] only produces a Chern number close to integer. The deviation in the finite difference numerical method is brought by finite grid points.

According to the perturbative expansion in Eq. (15), the Berry curvature (after tracing) is expected to be a constant in thermodynamic limit. Next, we examine the flatness of the Berry curvature under different system sizes. We define the following quantity to reflect the degree of flatness

$$f = \max \left\{ \text{Tr} [\tilde{\mathcal{F}}(\theta)] \right\} - \min \left\{ \text{Tr} [\tilde{\mathcal{F}}(\theta)] \right\}. \quad (38)$$

The numerical results are shown in Fig. 3 (c). It can be observed that the flatness of the Berry curvature tends to zero when $L \rightarrow \infty$, which is in accordance with our argument.

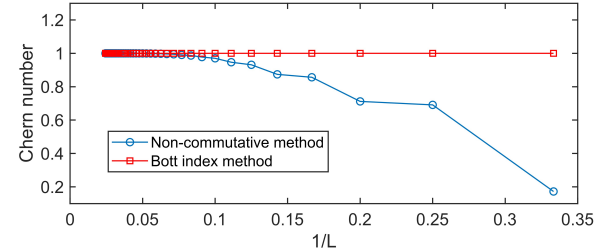


FIG. 4. Chern number as a function of system size calculated through the two real-space formulae (the non-commutative method [Eq. (21)] and the Bott index method [Eq. (33)]). Other parameters are set to: $t_1 = 1$, $t_2 = 0.5$ and $\Phi = \pi/2$.

B. Real-space Chern number in finite systems

In Sec. II B, we have seen that the real-space Chern number is based on the flatness of the Berry curvature defined through TBC. Nevertheless, the flat Berry curvature is only true in the thermodynamic limit. In finite systems, the Berry curvature may be dependent on twist angle, and therefore the real-space Chern number may deviate from the correct result. To see this effect, we

compute the Chern number using the real-space formulae [Eq. (21) and Eq. (33)] with different system sizes. For finite systems, we follow the idea proposed in Ref. [20, 23] to better approximate the finite difference of \tilde{P}_θ for the non-commutative Chern number. Detailed illustration of this higher-order finite difference method is presented in B. Numerical results are shown in Fig. 4. It can be seen that both methods tends to produce an integer number when $L \rightarrow \infty$.

It can be observed that the non-commutative method [Eq. (21)] is strongly affected by the system's size. This is because the non-commutative method relies on the flatness of Berry curvature. In Eq. (16), we only keep up to the linear terms of $1/L_j$, and regard the Berry curvature as a constant. Higher-order terms become considerable in finite systems, and the Berry curvature is not necessarily a constant, as already shown in previous subsection. To gain more accurate results through this method, one may take into account higher terms in the expansion of the projector \tilde{P}_θ , or increase the system's size.

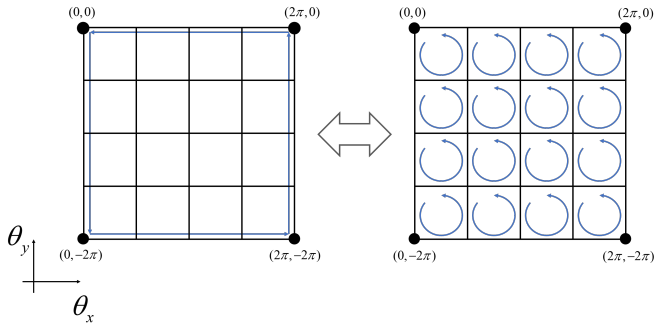


FIG. 5. The integral of Berry connection (indicated by blue arrows) defined through the TBC along the closed path \mathcal{D} is equivalent to the sum of integral in each small plaquette on the (θ_x, θ_y) plane.

On the other hand, it is surprising to observe that the Bott index method presents a very exact result $C = 1$ even for small size. In other words, the non-flatness of the Berry curvature will not affect the result of the Bott index. In fact, the Bott index in Eq. (33) is approximately related to the following path integral

$$\mathcal{U}_y^\dagger \mathcal{U}_x \mathcal{U}_y \mathcal{U}_x^\dagger \approx \exp \left(\oint_{\mathcal{D}} \tilde{\mathcal{A}}(\theta) \cdot d\theta \right), \quad (39)$$

where $\tilde{\mathcal{A}}(\theta) = (\tilde{\mathcal{A}}_x(\theta), \tilde{\mathcal{A}}_y(\theta))$, and $\mathcal{D} : (0,0) \rightarrow (0, -2\pi) \rightarrow (2\pi, -2\pi) \rightarrow (2\pi, 0) \rightarrow (0,0)$ is a closed path in (θ_x, θ_y) plane. With Stokes theorem, this integral is equivalent to the sum of the Berry curvature in Eq. (35), as depicted in Fig. 5. This means the Berry curvature is not necessarily flat when applying the Bott index method to calculate the Chern number in real space. In addition, one may recall that the Stokes theorem fails when Chern number is non-zero in topological band theory. This is because one can not find a globally smooth gauge for the Bloch state on the Brillouin manifold if the Chern

number is non-zero. Here, we instead consider gapped states Ψ_θ parameterized by twist angle and use the non-Abelian form of the Berry connection. There is no obstruction in applying the Stokes theorem, which explains why the Bott index produces an exactly quantized Chern number.

C. Chern number in the presence of disorder

As mentioned in previous sections, the real-space formula allows us to compute the Chern number without requiring the translation symmetry. To examine this fact, we consider on-site energy disorder on each site's in Haldane model

$$\hat{H} = \hat{H}_0 + W \sum_r \epsilon_r \hat{n}_r \quad (40)$$

where W is the strength of the disorder, and $\epsilon_r \in [-0.5, 0.5]$ is a uniformly distributed random number. We numerically diagonalize the Hamiltonian under PBC and focus on the lowest band. The parameter is chosen to be $t_1 = 1$, $t_2 = 0.5$, $\Phi = \pi/2$, corresponding to the $C = 1$ topological phase in the clean system. Then, we increase the strength of the disorder, and the topological band theory fails in this situation. By employing the real-space formula (the non-commutative method [Eq. (21)] and the Bott index method [Eq. (33)]), we compute the Chern number as a function of disorder strength W , see results in Fig. 6. The result is averaged over 500 random realizations. It can be seen that the Chern number remains $C = 1$ for moderate disorder and then there appears a disorder-induced topological transition for stronger disorder. One can find that results from the two real-space Chern number are well consistent, despite some differences due to the finite-size effect. As expected, the Bott index method will exactly produce an integer for all realizations, while the non-commutative method will give a non-quantized result near the phase transition point. These two methods are expected to be equivalent in the thermodynamic limit.

IV. CONCLUSIONS AND DISCUSSIONS

In summary, in the thermodynamic limit, we have shown that the non-commutative Chern number and the Bott index form of Chern number can be both derived from the Chern number defined via TBC. Thus, these two real-space formulae and the TBC formula for the Chern number are equivalent. Our derivation is based on the perturbative nature of the twist angles under the uniform gauge of TBC. The key point is to expand the eigenstate and operator to the linear terms of $1/L_x$ and $1/L_y$. The trace of non-Abelian Berry curvature is shown to be a constant in the thermodynamic limit. Hence, the integration w.r.t. twist angles in the TBC Chern number will be reduced, providing feasibility to deriving the

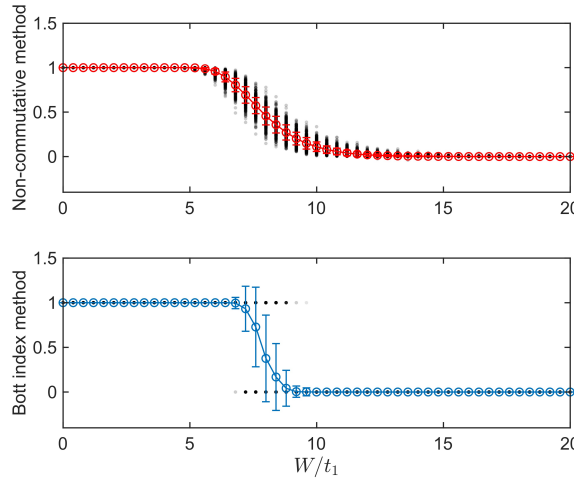


FIG. 6. Numerical computations of the real-space Chern number as a function of disorder strength W on a $L_x \times L_y = 30 \times 30$ system. Grey points are from each random realization, while circles are the averaged results. We have performed computations over 500 random realizations. The errorbar represents the standard deviations of Chern numbers among these random realizations. Other parameters are set to $t_1 = 1$, $t_2 = 0.5$, $\Phi = \pi/2$.

real-space Chern number. The flatness of the trace of Berry curvature defined via TBC is later verified numerically. The non-flatness effect to the real-space formula of Chern number is discussed. We also show that the real-space Chern number can be applied to disordered system. We would like to stress that using the formula of topological invariants defined via TBC to derive the real-space topological invariant may be also generalized to other systems, such as higher-order topological insulators [18, 53] and periodically-driven systems in 2D [54]. This will benefit the search of real-space formula of topological invariants.

Throughout this paper, we restrict ourself to the single-particle system. In fact, the TBC method can be well applied to gapped many-body eigenstates. Since the real-space formulae of Chern number can be derived from the TBC Chern number, we expect the real-space Chern number can be extended to multi-particle systems. However, it seems that the Bott index can not work for unique many-body ground state $|\Psi_{\text{GS}}\rangle$ because $\mathcal{U}_{x,y}$ is only a U(1) number in this case. Hence, Eq. (33) will only produce a trivial result due to the multi-value nature of the exponential function in \mathbb{C} . In other words, one can not numerically distinguish trivial and non-trivial topological insulators through the Bott index formula if the ground state is unique. To circumvent this problem, we recall that the Bott index can be considered as a integral of Berry connection, as mentioned in Fig. 5. Hence, it is possible to implement the integral for half of the area under TBC with uniform gauge, that is the triangle region $\mathcal{D}' : (0,0) \rightarrow (0,-2\pi) \rightarrow (2\pi,-2\pi) \rightarrow (0,0)$. This

leads to the following expression

$$\begin{aligned} \tilde{C}_{\text{TBC}} &\approx \frac{1}{i\pi} \log \langle \tilde{\Psi}_{\text{GS}}(0,0) | \tilde{\Psi}_{\text{GS}}(0,-2\pi) \rangle \\ &\quad \times \langle \tilde{\Psi}_{\text{GS}}(0,-2\pi) | \tilde{\Psi}_{\text{GS}}(2\pi,-2\pi) \rangle \\ &\quad \times \langle \tilde{\Psi}_{\text{GS}}(2\pi,-2\pi) | \tilde{\Psi}_{\text{GS}}(0,0) \rangle \\ &= \frac{1}{i\pi} \log \langle \Psi_{\text{GS}} | \left(\hat{U}_{2\pi}^y \right)^{-1} | \Psi_{\text{GS}} \rangle \langle \Psi_{\text{GS}} | \hat{U}_{2\pi}^x | \Psi_{\text{GS}} \rangle \\ &\quad \times \langle \Psi_{\text{GS}} | \left(\hat{U}_{2\pi}^x \right)^{-1} \hat{U}_{2\pi}^y | \Psi_{\text{GS}} \rangle, \end{aligned} \quad (41)$$

which is quite similar to the real-space marker of the Chern insulator proposed recently in Ref. [55, 56]. In addition, it should be noted that this quantity also relies on the flatness of the Berry curvature, and it is not necessarily quantized in finite systems. We only expect it to be quantized in the thermodynamic limit.

As for the non-commutative method [Eq. (21)], we can consider a more fundamental formula described in Eq. 16 for better approximation, which yields

$$\tilde{C}_{\text{TBC}} \approx -2\pi i \langle \Psi_{\text{GS}} | \left[\left(\partial_{\theta_x} \tilde{P}_{\theta} \right) \Big|_{\theta=0}, \left(\partial_{\theta_y} \tilde{P}_{\theta} \right) \Big|_{\theta=0} \right] | \Psi_{\text{GS}} \rangle. \quad (42)$$

By using finite difference to approximate the partial derivative, one is also able to obtain an approximated Chern number.

Finally, we remark that the real-space formula of Chern number introduced in this work may not apply to the \mathbb{Z}_2 topological insulator (i.e. the quantum spin Hall insulator [57]) since the total Chern number is always zero. Nevertheless, we note that it is still possible to appropriately modify the TBC in this system [58] to define the spin Chern number. Hence, it is desirable to investigate the real-space Chern number in \mathbb{Z}_2 topological insulators. We shall left this part in the future works.

ACKNOWLEDGMENTS

This work is supported by the National Key Research and Development Program of China (Grant No. 2022YFA1404104), and the National Natural Science Foundation of China (Grant No. 12025509, 12247134).

Appendix A: Invariance of Chern number under different gauges

We would like to prove that the formulae of TBC Chern number under the boundary gauge and uniform gauge have the same form. According to Eq. (6), there is $\tilde{\Psi}_{\theta} = \hat{U}_{\theta} \Psi_{\theta}$. Then, we find the Berry connection is

transformed as

$$\begin{aligned}
\tilde{\mathcal{A}}_j(\boldsymbol{\theta}) &= \tilde{\Psi}_{\boldsymbol{\theta}}^\dagger \partial_{\theta_j} \tilde{\Psi}_{\boldsymbol{\theta}} \\
&= \Psi_{\boldsymbol{\theta}}^\dagger \hat{U}_{\boldsymbol{\theta}}^{-1} \partial_{\theta_j} (\hat{U}_{\boldsymbol{\theta}} \Psi_{\boldsymbol{\theta}}) \\
&= \Psi_{\boldsymbol{\theta}}^\dagger \partial_{\theta_j} \Psi_{\boldsymbol{\theta}} + \Psi_{\boldsymbol{\theta}}^\dagger (\hat{U}_{\boldsymbol{\theta}}^{-1} \partial_{\theta_j} \hat{U}_{\boldsymbol{\theta}}) \Psi_{\boldsymbol{\theta}} \\
&= \mathcal{A}_j(\boldsymbol{\theta}) + \Psi_{\boldsymbol{\theta}}^\dagger \frac{\hat{r}_j}{L_j} \Psi_{\boldsymbol{\theta}}, \quad j = x, y. \quad (\text{A1})
\end{aligned}$$

Hence, it can be found that the Berry curvature satisfies

$$\tilde{\mathcal{F}}(\boldsymbol{\theta}) = \mathcal{F}(\boldsymbol{\theta}) + [\partial_{\theta_y} \bar{r}_x(\boldsymbol{\theta}) - \partial_{\theta_x} \bar{r}_y(\boldsymbol{\theta})], \quad (\text{A2})$$

where we denote $\bar{r}_j(\boldsymbol{\theta}) \equiv \Psi_{\boldsymbol{\theta}}^\dagger \frac{\hat{r}_j}{L_j} \Psi_{\boldsymbol{\theta}}$ for simplicity. It can be seen that generally $\tilde{\mathcal{F}}(\boldsymbol{\theta}) \neq \mathcal{F}(\boldsymbol{\theta})$. Note that, when the twist angle changes a flux quanta, which is 2π here, the system returns to the origin. Meanwhile, it can be immediately checked that $\bar{r}_j(\boldsymbol{\theta})$ is a single-value and gauge-invariant periodic function of twist angle. Hence, there should be

$$\text{Tr}[\bar{r}_j(\boldsymbol{\theta} + 2\pi \mathbf{e}_{j'})] = \text{Tr}[\bar{r}_j(\boldsymbol{\theta})], \quad j, j' = x, y, \quad (\text{A3})$$

where $\mathbf{e}_{j'}$ represents the unit vector along $j' = x, y$ direction. After integrating over twist angles, there is

$$\int_0^{2\pi} \int_0^{2\pi} d\theta_x d\theta_y \text{Tr}[\partial_{\theta_{j'}} \bar{r}_j(\boldsymbol{\theta})] = 0, \quad j, j' = x, y. \quad (\text{A4})$$

Thus, we can conclude that the Chern number defined through TBC is the same under the boundary gauge and the uniform gauge. In other words, the large gauge transformation in Eq. (6) will not affect the Chern number.

Appendix B: Approximation for finite difference

To better approximate the partial derivative of the projector matrix numerically, one can use a higher-order finite difference method for this first-order derivative introduced in Ref. [20, 23]. To see how it works, we write down series expansion of the projector with respect to θ/L :

$$P_{\theta/L} = P_0 + \sum_{k=1}^{\infty} \left(\frac{\theta}{L}\right)^k \frac{1}{k!} \left[\frac{\partial^k}{\partial(\theta/L)^k} P_{\theta/L} \right]_{\theta=0}. \quad (\text{B1})$$

As a demonstration, we assume that the projector is only parameterized by θ . The result can be readily extended to the 2D system discussed in the main text. By construction, there is

$$\begin{aligned}
\frac{P_{\theta/L} - P_{-\theta/L}}{2} &= \sum_{m=1}^{\infty} \left(\frac{\theta}{L}\right)^{2m-1} \frac{1}{(2m-1)!} \\
&\quad \times \left[\frac{\partial^{2m-1}}{\partial(\theta/L)^{2m-1}} P_{\theta/L} \right]_{\theta=0}. \quad (\text{B2})
\end{aligned}$$

Thus, by choosing a set of parameters $\{c_n\}$ to eliminate higher-order terms, the first-order derivative can be written as

$$\frac{\theta}{L} \left[\frac{\partial}{\partial(\theta/L)} P_{\theta/L} \right]_{\theta=0} \approx \sum_{n \in \mathbb{Z}^+} \frac{c_n}{2} (P_{n\theta/L} - P_{-n\theta/L}) \quad (\text{B3})$$

The coefficient $\{c_n\}$ can be solved through a set of linear equations according to the series expansion. By truncating the expansion to Q terms with $Q < L/2$ (to ensure the convergence of the expansion), it can be written in a matrix form

$$\begin{pmatrix} c_1 & c_2 & \cdots & c_Q \end{pmatrix} \begin{pmatrix} P_{\theta/L} - P_{-\theta/L} \\ P_{2\theta/L} - P_{-2\theta/L} \\ \vdots \\ P_{Q\theta/L} - P_{-Q\theta/L} \end{pmatrix} \times \frac{1}{2} = \frac{\theta}{L} \left[\frac{\partial}{\partial(\theta/L)} P_{\theta/L} \right]_{\theta=0}. \quad (\text{B4})$$

Then, we can convert this problem to solving a set of linear equations, which can be expressed as

$$\begin{pmatrix} 1 & 2 & \cdots & Q \\ 1^3 & 2^3 & \cdots & Q^3 \\ \vdots & \vdots & \ddots & \vdots \\ 1^{2Q-1} & 2^{2Q-1} & \cdots & Q^{2Q-1} \end{pmatrix} \begin{pmatrix} c_1 \\ c_2 \\ \vdots \\ c_Q \end{pmatrix} = \begin{pmatrix} 1 \\ 0 \\ \vdots \\ 0 \end{pmatrix} \quad (\text{B5})$$

Hence, by taking the matrix inverse, $\{c_n\}$ can be solved numerically through:

$$\begin{pmatrix} c_1 \\ c_2 \\ \vdots \\ c_Q \end{pmatrix} = \begin{pmatrix} 1 & 2 & \cdots & Q \\ 1^3 & 2^3 & \cdots & Q^3 \\ \vdots & \vdots & \ddots & \vdots \\ 1^{2Q-1} & 2^{2Q-1} & \cdots & Q^{2Q-1} \end{pmatrix}^{-1} \begin{pmatrix} 1 \\ 0 \\ \vdots \\ 0 \end{pmatrix}. \quad (\text{B6})$$

Next, by using the fact that

$$P_{2n\pi/L} = (\hat{U}_{2\pi})^n P_0 (\hat{U}_{-2\pi})^n \quad (\text{B7})$$

we can let $\theta = 2\pi$ and then:

$$\begin{aligned}
&\frac{2\pi}{L} \left[\frac{\partial}{\partial(\theta/L)} P_{\theta/L} \right]_{\theta=0} \\
&\approx \sum_{n=1}^Q \frac{c_n}{2} \left[(\hat{U}_{2\pi})^n P_0 (\hat{U}_{-2\pi})^n - (\hat{U}_{-2\pi})^n P_0 (\hat{U}_{2\pi})^n \right], \quad (\text{B8})
\end{aligned}$$

which can be evaluated numerically and produces a good approximation for the partial derivative.

Appendix C: Quasi-unitarity of the matrices $\mathcal{U}_{x,y}$

Below, we show that the matrix $\mathcal{U}_j = \Psi_0^\dagger \hat{U}_{2\pi}^j \Psi_0$, $j = x, y$ mentioned in the main text is a unitary matrix in the

thermodynamic limit $L_j \rightarrow \infty$ through the TBC. Firstly, note that

$$\mathcal{U}_j = \Psi_0^\dagger \hat{U}_{2\pi}^j \Psi_0, \quad \mathcal{U}_j^\dagger = \Psi_0^\dagger (\hat{U}_{2\pi}^j)^{-1} \Psi_0. \quad (\text{C1})$$

The vector is normalized: $\Psi_0^\dagger \Psi_0 = I_{\mathcal{N}}$, and \mathcal{N} is the number of targeted states. Meanwhile, we have $\Psi_0 \Psi_0^\dagger = \sum_{\mu \in \text{target}} |\psi_\mu(0)\rangle \langle \psi_\mu(0)| = 1$ in the subspace spanned by targeted states without the TBC. There is

$$\begin{aligned} \mathcal{U}_{2\pi}^j (\mathcal{U}_{2\pi}^j)^\dagger &= \Psi_0^\dagger \hat{U}_{2\pi}^j \Psi_0 \Psi_0^\dagger (\hat{U}_{2\pi}^j)^{-1} \Psi_0 \\ &= \Psi_0^\dagger \hat{U}_{2\pi}^j \left(\sum_\mu |\psi_\mu(0)\rangle \langle \psi_\mu(0)| \right) (\hat{U}_{2\pi}^j)^{-1} \Psi_0 \\ &= \Psi_0^\dagger \left(\sum_\mu |\tilde{\psi}_\mu(2\pi e_j)\rangle \langle \tilde{\psi}_\mu(2\pi e_j)| \right) \Psi_0. \end{aligned} \quad (\text{C2})$$

Approximately, there is

$$\begin{aligned} \sum_\mu |\psi_\mu(\theta)\rangle \langle \psi_\mu(\theta)| &= \sum_\mu |\psi_\mu\rangle \langle \psi_\mu| + O\left(\frac{1}{L}\right) \\ &= 1 + O\left(\frac{1}{L}\right) \end{aligned} \quad (\text{C3})$$

which implies that $\sum_{\mu \in \text{target}} |\psi_\mu(2\pi)\rangle \langle \psi_\mu(2\pi)|$ is close to the identity matrix in this subspace. Hence, we find $\mathcal{M}\mathcal{M}^\dagger = I_{\mathcal{N}}$ in the thermodynamic limit. One can also prove that $\mathcal{M}^\dagger \mathcal{M} = I_{\mathcal{N}}$ using the same analysis. In summary, we have shown that the matrix \mathcal{M} is approximately a unitary matrix in the thermodynamic limit. Similar conclusions can be found in Refs. [26, 27].

Appendix D: Derivations of Eq. (27)

Here we show that how to derive the partial derivative of the Berry phase formulated by projected position

operator. The projected position operator reads as

$$\tilde{P}_{(\theta_x,0)} \hat{U}_{2\pi}^y \tilde{P}_{(\theta_x,0)} = \sum_{\mu,\mu' \in \text{target}} [\mathcal{U}_y(\theta_x)]_{\mu,\mu'} |\psi_\mu(\theta_x)\rangle \langle \psi_{\mu'}(\theta_x)|. \quad (\text{D1})$$

One can diagonalize the matrix $\mathcal{U}_y(\theta_x)$ to find

$$\tilde{P}_{(\theta_x,0)} \hat{U}_{2\pi}^y \tilde{P}_{(\theta_x,0)} = \sum_n e^{i\Phi_n(\theta_x)} |\Phi_n(\theta_x)\rangle \langle \Phi_n(\theta_x)|, \quad (\text{D2})$$

where we assumed $\mathcal{U}_y(\theta_x)$ is unitary and hence its eigenvalues are $U(1)$ numbers. Then, the logarithm of the projected position operator can be equivalently expressed as

$$\log [\tilde{P}_{(\theta_x,0)} \hat{U}_{2\pi}^y \tilde{P}_{(\theta_x,0)}] = i \sum_n \Phi_n(\theta_x) |\Phi_n(\theta_x)\rangle \langle \Phi_n(\theta_x)|. \quad (\text{D3})$$

Taking the partial derivative yields

$$\begin{aligned} \frac{\partial}{\partial \theta_x} \log [\tilde{P}_{(\theta_x,0)} \hat{U}_{2\pi}^x \tilde{P}_{(\theta_x,0)}] \\ = i \sum_n \left[\frac{\partial}{\partial \theta_x} \Phi_n(\theta_x) \right] |\Phi_n(\theta_x)\rangle \langle \Phi_n(\theta_x)| \\ + i \sum_n \Phi_n(\theta_x) \frac{\partial}{\partial \theta_x} [|\Phi_n(\theta_x)\rangle \langle \Phi_n(\theta_x)|]. \end{aligned} \quad (\text{D4})$$

The second term will vanish under the trace operation, and then we have

$$\text{Tr} \left\{ \frac{\partial}{\partial \theta_x} \log [\tilde{P}_{(0,\theta_x)} \hat{U}_{2\pi}^x \tilde{P}_{(0,\theta_x)}] \right\} = i \sum_n \frac{\partial}{\partial \theta_x} \Phi_n(\theta_x). \quad (\text{D5})$$

Note that, in band insulator, $\Phi_n(\theta_x)$ is proportional to the center of Wannier function. In the same vein, one can find that

$$\begin{aligned} \text{Tr} \left\{ \left[\tilde{P}_{(\theta_x,0)} \left(\hat{U}_{2\pi}^y \right)^{-1} \tilde{P}_{(\theta_x,0)} \right] \frac{\partial}{\partial \theta_x} [\tilde{P}_{(0,\theta_x)} \hat{U}_{2\pi}^y \tilde{P}_{(0,\theta_x)}] \right\} \\ = i \sum_n \frac{\partial}{\partial \theta_x} \Phi_n(\theta_x) \\ = \text{Tr} \left\{ \frac{\partial}{\partial \theta_x} \log [\tilde{P}_{(\theta_x,0)} \hat{U}_{2\pi}^y \tilde{P}_{(\theta_x,0)}] \right\}, \end{aligned} \quad (\text{D6})$$

which gives rise to Eq. (27).

[1] M. Z. Hasan and C. L. Kane, Colloquium: Topological insulators, *Rev. Mod. Phys.* **82**, 3045 (2010).
[2] X.-L. Qi and S.-C. Zhang, Topological insulators and superconductors, *Rev. Mod. Phys.* **83**, 1057 (2011).
[3] C. L. Kane, Topological band theory and the \mathbb{Z}_2 invariant, *Contemporary Concepts of Condensed Matter Science*, **6**, 3 (2013).
[4] C.-K. Chiu, J. C. Y. Teo, A. P. Schnyder, and S. Ryu, Classification of topological quantum matter with symmetries, *Rev. Mod. Phys.* **88**, 035005 (2016).
[5] D. J. Thouless, M. Kohmoto, M. P. Nightingale, and M. den Nijs, Quantized Hall Conductance in a Two-Dimensional Periodic Potential, *Phys. Rev. Lett.* **49**, 405 (1982).
[6] Q. Niu and D. J. Thouless, Quantised adiabatic charge transport in the presence of substrate disorder and many-body interaction, *Journal of Physics A: Mathematical and General* **17**, 2453 (1984).
[7] R. Tao and Y.-S. Wu, Gauge invariance and fractional quantum hall effect, *Phys. Rev. B* **30**, 1097 (1984).

[8] Q. Niu, D. J. Thouless, and Y.-S. Wu, Quantized Hall conductance as a topological invariant, *Phys. Rev. B* **31**, 3372 (1985).

[9] D. Xiao, M.-C. Chang, and Q. Niu, Berry phase effects on electronic properties, *Rev. Mod. Phys.* **82**, 1959 (2010).

[10] Z. Gong, Y. Ashida, K. Kawabata, K. Takasan, S. Higashikawa, and M. Ueda, Topological Phases of Non-Hermitian Systems, *Phys. Rev. X* **8**, 031079 (2018).

[11] L. Lin, Y. Ke, and C. Lee, Real-space representation of the winding number for a one-dimensional chiral-symmetric topological insulator, *Phys. Rev. B* **103**, 224208 (2021).

[12] R. B. Laughlin, Quantized hall conductivity in two dimensions, *Phys. Rev. B* **23**, 5632 (1981).

[13] M. Oshikawa and T. Senthil, Fractionalization, topological order, and quasiparticle statistics, *Phys. Rev. Lett.* **96**, 060601 (2006).

[14] Y. Huo and R. N. Bhatt, Current carrying states in the lowest landau level, *Phys. Rev. Lett.* **68**, 1375 (1992).

[15] J. E. Avron and R. Seiler, Quantization of the hall conductance for general, multiparticle schrödinger hamiltonians, *Phys. Rev. Lett.* **54**, 259 (1985).

[16] Q. Niu, Theory of the quantized adiabatic particle transport, *Modern Physics Letters B* **5**, 923 (1991).

[17] H. Watanabe and M. Oshikawa, Inequivalent berry phases for the bulk polarization, *Phys. Rev. X* **8**, 021065 (2018).

[18] J. F. Wienand, F. Horn, M. Aidelsburger, J. Bibo, and F. Grusdt, Thouless pumps and bulk-boundary correspondence in higher-order symmetry-protected topological phases, *Phys. Rev. Lett.* **128**, 246602 (2022).

[19] L. Lin, Y. Ke, and C. Lee, Topological invariants for interacting systems: From twisted boundary conditions to center-of-mass momentum, *Phys. Rev. B* **107**, 125161 (2023).

[20] E. Prodan, T. L. Hughes, and B. A. Bernevig, Entanglement Spectrum of a Disordered Topological Chern Insulator, *Phys. Rev. Lett.* **105**, 115501 (2010).

[21] E. Prodan, Robustness of the spin-chern number, *Phys. Rev. B* **80**, 125327 (2009).

[22] E. Prodan, Non-commutative tools for topological insulators, *New Journal of Physics* **12**, 065003 (2010).

[23] E. Prodan, Disordered topological insulators: a non-commutative geometry perspective, *Journal of Physics A: Mathematical and Theoretical* **44**, 113001 (2011).

[24] E. Prodan, *A computational non-commutative geometry program for disordered topological insulators*, Vol. 23 (Springer, 2017).

[25] R. Exel and T. A. Loring, Invariants of almost commuting unitaries, *Journal of Functional Analysis* **95**, 364 (1991).

[26] T. A. Loring and M. B. Hastings, Disordered topological insulators via C^* -algebras, *EPL (Europhysics Letters)* **92**, 67004 (2010).

[27] M. B. Hastings and T. A. Loring, Almost commuting matrices, localized Wannier functions, and the quantum Hall effect, *Journal of mathematical physics* **51**, 015214 (2010).

[28] M. B. Hastings and T. A. Loring, Topological insulators and C^* -algebras: Theory and numerical practice, *Annals of Physics* **326**, 1699 (2011), july 2011 Special Issue.

[29] T. A. Loring, K-theory and pseudospectra for topological insulators, *Annals of Physics* **356**, 383 (2015).

[30] I. Mondragon-Shem, T. L. Hughes, J. Song, and E. Prodan, Topological Criticality in the Chiral-Symmetric AIII Class at Strong Disorder, *Phys. Rev. Lett.* **113**, 046802 (2014).

[31] J. E. Avron, R. Seiler, and B. Simon, Homotopy and quantization in condensed matter physics, *Phys. Rev. Lett.* **51**, 51 (1983).

[32] M. Yamanaka, M. Oshikawa, and I. Affleck, Nonperturbative approach to luttinger's theorem in one dimension, *Phys. Rev. Lett.* **79**, 1110 (1997).

[33] H. Watanabe, Insensitivity of bulk properties to the twisted boundary condition, *Phys. Rev. B* **98**, 155137 (2018).

[34] J. Bellissard, Noncommutative geometry and quantum hall effect, in *Proceedings of the International Congress of Mathematicians: August 3–11, 1994 Zürich, Switzerland* (Springer, 1995) pp. 1238–1246.

[35] E. Prodan, B. Leung, and J. Bellissard, The non-commutative nth-chern number ($n \geq 1$), *Journal of Physics A: Mathematical and Theoretical* **46**, 485202 (2013).

[36] C. Bourne and E. Prodan, Non-commutative chern numbers for generic aperiodic discrete systems, *Journal of Physics A: Mathematical and Theoretical* **51**, 235202 (2018).

[37] K. Kudo, H. Watanabe, T. Kariyado, and Y. Hatsugai, Many-body chern number without integration, *Phys. Rev. Lett.* **122**, 146601 (2019).

[38] T. A. Loring, A guide to the bott index and localizer index, arXiv preprint arXiv:1907.11791 10.48550/arXiv.1907.11791 (2019).

[39] M. A. Bandres, M. C. Rechtsman, and M. Segev, Topological Photonic Quasicrystals: Fractal Topological Spectrum and Protected Transport, *Phys. Rev. X* **6**, 011016 (2016).

[40] A. Agarwala and V. B. Shenoy, Topological insulators in amorphous systems, *Phys. Rev. Lett.* **118**, 236402 (2017).

[41] H. Huang and F. Liu, Quantum spin hall effect and spin bott index in a quasicrystal lattice, *Phys. Rev. Lett.* **121**, 126401 (2018).

[42] H. Huang and F. Liu, Theory of spin bott index for quantum spin hall states in nonperiodic systems, *Phys. Rev. B* **98**, 125130 (2018).

[43] X. S. Wang, A. Brataas, and R. E. Troncoso, Bosonic bott index and disorder-induced topological transitions of magnons, *Phys. Rev. Lett.* **125**, 217202 (2020).

[44] P. Titum, N. H. Lindner, M. C. Rechtsman, and G. Refael, Disorder-induced floquet topological insulators, *Phys. Rev. Lett.* **114**, 056801 (2015).

[45] D. Toniolo, On the bott index of unitary matrices on a finite torus, *Letters in Mathematical Physics* **112**, 126 (2022).

[46] H. Dehghani, Z.-P. Cian, M. Hafezi, and M. Barkeshli, Extraction of the many-body chern number from a single wave function, *Phys. Rev. B* **103**, 075102 (2021).

[47] Z.-P. Cian, H. Dehghani, A. Elben, B. Vermersch, G. Zhu, M. Barkeshli, P. Zoller, and M. Hafezi, Many-body chern number from statistical correlations of randomized measurements, *Phys. Rev. Lett.* **126**, 050501 (2021).

[48] B. Kang, W. Lee, and G. Y. Cho, Many-body invariants for chern and chiral hinge insulators, *Phys. Rev. Lett.* **126**, 016402 (2021).

- [49] F. D. M. Haldane, Model for a Quantum Hall Effect without Landau Levels: Condensed-Matter Realization of the "Parity Anomaly", *Phys. Rev. Lett.* **61**, 2015 (1988).
- [50] G. Jotzu, M. Messer, R. Desbuquois, M. Lebrat, T. Uehlinger, D. Greif, and T. Esslinger, Experimental realization of the topological haldane model with ultracold fermions, *Nature* **515**, 237 (2014).
- [51] N. Fläschner, D. Vogel, M. Tarnowski, B. Rem, D.-S. Lühmann, M. Heyl, J. Budich, L. Mathey, K. Sengstock, and C. Weitenberg, Observation of dynamical vortices after quenches in a system with topology, *Nature Physics* **14**, 265 (2018).
- [52] T. Fukui, Y. Hatsugai, and H. Suzuki, Chern numbers in discretized brillouin zone: Efficient method of computing (spin) hall conductances, *Journal of the Physical Society of Japan* **74**, 1674 (2005), <https://doi.org/10.1143/JPSJ.74.1674>.
- [53] W. A. Benalcazar and A. Cerjan, Chiral-symmetric higher-order topological phases of matter, *Phys. Rev. Lett.* **128**, 127601 (2022).
- [54] M. S. Rudner, N. H. Lindner, E. Berg, and M. Levin, Anomalous edge states and the bulk-edge correspondence for periodically driven two-dimensional systems, *Phys. Rev. X* **3**, 031005 (2013).
- [55] I. Gilardonni, F. Becca, A. Marrazzo, and A. Parola, Real-space many-body marker for correlated F_2 topological insulators, *Phys. Rev. B* **106**, L161106 (2022).
- [56] Y.-C. Tzeng, P.-Y. Chang, and M.-F. Yang, Interaction-induced metal to topological insulator transition, *Phys. Rev. B* **107**, 155106 (2023).
- [57] C. L. Kane and E. J. Mele, Quantum Spin Hall Effect in Graphene, *Phys. Rev. Lett.* **95**, 226801 (2005).
- [58] X.-L. Qi, Y.-S. Wu, and S.-C. Zhang, General theorem relating the bulk topological number to edge states in two-dimensional insulators, *Phys. Rev. B* **74**, 045125 (2006).